Korean J. Chem. Eng., **26**(5), 1235-1240 (2009)
DOI: 10.1007/s11814-009-0199-2

Direct incorporation of vanadium into three-dimensional KIT-6: 1. Optimization of synthesis conditions

Balasamy Rabindran Jermy, Sang-Yun Kim, Kanattukara Vijayan Bineesh, Manickam Selvaraj, and Dae-Won Park†

Division of Chemical Engineering, Pusan National University, Busan 609-735, Korea
(*Received 14 November 2008 • accepted 7 February 2009*)

Abstract−Three dimensional (3-D) cubic KIT-6 with directly incorporated vanadium was hydrothermally synthesized by using Pluronic P123 and *n*-butanol as the structure-directing mixture, tetraethyl orthosilicate (TEOS) as the silica source and NH_4VO_3 as the vanadium source. The molar composition was varied in the range of 0.017 P123/0.08-2.4 V/1.0-2.0 TEOS/1.31-1.70 BuOH/1.83-3.00 HCl/195 H_2O. The orderness of mesopore structure was estimated by X-ray diffraction, N_2 adsorption, and TEM analysis. The effects of the amount of HCl, TEOS and BuOH on the structure of KIT-6 were discussed. The time and temperature for the synthesis of KIT-6 were also optimized. The amount of vanadium content influenced the framework structure and crystallinity of the Ia3d phase significantly.

Key words: KIT-6, Hydrothermal Synthesis, Vanadium Incorporation

INTRODUCTION

The incorporation of vanadium into mesoporous molecular sieves is of considerable interest for catalytic applications. However, most studies have dealt with the one-dimensional hexagonal MCM-41 [1,2]. A more complete characterization of the coordination of vanadium containing mesoporous MCM-41 molecular sieves was reported by Gontier and Tuel [3]. They noticed that the V center of calcined and as-synthesized V-MCM-41 had the same coordination state, with no direct chemical bonding to the silicate framework. Optimization of the synthesis of the hexagonal SBA-15, and its catalytic activation [4], has attracted considerable attention over the past few years. Despite its potential, there are only few reports on the direct incorporation of vanadium into SBA-15 materials [5,6]. This is due to the difficulty in introducing the metal ions into SBA-15 as a result of the facile dissociation of metal-O-Si bonds under strongly acidic hydrothermal conditions. Therefore, several studies have dealt with the incorporation of metal ions into SBA-15 using solely post synthetic grafting methods. Nevertheless, there are disadvantages with this process, such as extra-framework species and irregularly distributed active sites that eventually lead to the decrease in the specific surface area, pore volume, and pore diameter [7].

Large-pore three-dimensional (3D) mesoporous silica materials are among the most interesting mesoporous materials for potential applications requiring easily accessible and uniform large pores. Examples of these are SBA-15 (*p6mm*) [8] and SBA-16 (*Im3m*) [9], which have cylindrical and cage type structures, respectively. However, the phase transformation from a cubic phase into a hexagonal phase occurred when a high metal content was incorporated [10]. Quite recently, large-pore mesoporous KIT-6 silicas with a cubic Ia3d structure were synthesized using triblock copolymers under various synthesis conditions [11]. This material consists of a three-dimensional (3-D) cubic Ia3d mesostructure with two interpenetrating continuous networks of chiral channels. This unique 3-D channel network is believed to provide a highly opened porous host with easy and direct access for guest species, thereby facilitating inclusion or diffusion throughout the pore channels without pore blockage. Despite this advantage only little work has been done on metal-substituted KIT-6 materials. To understand the influence of a metal on the characteristics of KIT-6, a detailed study was carried out on the optimization conditions of vanadium incorporation adhering to the limited phase domain reported by Ryoo et al. [11].

EXPERIMENTAL

1. Synthesis of Materials

The V-KIT-6 materials were prepared by using a Pluronic P123 and *n*-butanol as the structure-directing mixture, TEOS (Aldrich, 98%) as the silica source and NH_4VO_3 (Aldrich, 99.9%) as the vanadium source. The molar composition was varied in the range of (0.017 P123/0.08-2.4 V/1.0-2.0 TEOS/1.31-1.70 BuOH/1.83-3.00 HCl/195 H_2O). 4.0 g of P123 and 7.4 g of 37 wt% HCl were dissolved in 144 g of distilled water. After complete dissolution, 4.0 g of BuOH was added. Then, 8.6 g of TEOS along with the required amount of vanadium was added simultaneously to the homogeneous clear solution. The resulting mixture was stirred vigorously at 353-403 K for 24-48 h. The precipitated product was filtered, washed thoroughly and dried for 24 h. The obtained material was calcined in a programmable oven (298-823 K; heating rate 1 °C/min) for 8 h in a N_2 and 8 h in an air atmosphere.

2. Characterization

X-ray diffraction (XRD, Philips X′pert PRO MRD system) was carried out using nickel filtered CuKα radiation (λ=1.5406 Å). The metal content in the KIT-6 was measured by inductively coupled plasma optical emission spectrometer (ICP-OES, JOBIN YVON) and X-ray fluorescence spectroscopy (XRF, Philips PW 2400). The surface area, pore volume and pore size distribution were meas-

†To whom correspondence should be addressed.
E-mail: dwpark@pusan.ac.kr

ured by nitrogen adsorption apparatus (ASAP-2010, Micromeritics). High-resolution transmission electron microscopy (HRTEM) imaging was performed with a JEOL CM 30 ST electron microscope operated at 200 kV.

RESULTS AND DISCUSSION

In general, the syntheses of vanadium-incorporated mesoporous molecular sieves were performed over relatively longer synthesis times [12-16]. Hitherto, the amount of vanadium really substituted was very low. Efforts were made to incorporate a high V content into the cubic mesophase of KIT-6 at shorter period. Ryoo et al. [11] reported a detailed study of the synthesis of a high quality siliceous KIT-6 material using the gel with molar ratio of 0.017 P123/1.0 TEOS/1.31 BuOH/1.83 HCl/195 H_2O. When we attempted to synthesize V-KIT-6 directly with an Si/V ratio of 30 in a synthesis gel under the same condition, the cubic phase slaked without a minimum degree of cubic mesoscopic order (Fig. 1(a)). Without optimization, the incorporation of metal appears to show a negative effect on the complex interconnected pores. Therefore, for the optimization of the synthesis conditions, KIT-6 with a fixed Si/V ratio of 65 was chosen, and the molar ratio of HCl, TEOS, and BuOH were varied as 1.83-3.0/1.0-2.0/1.31-1.70, respectively. The synthesis was carried out at 373 K for 24 h.

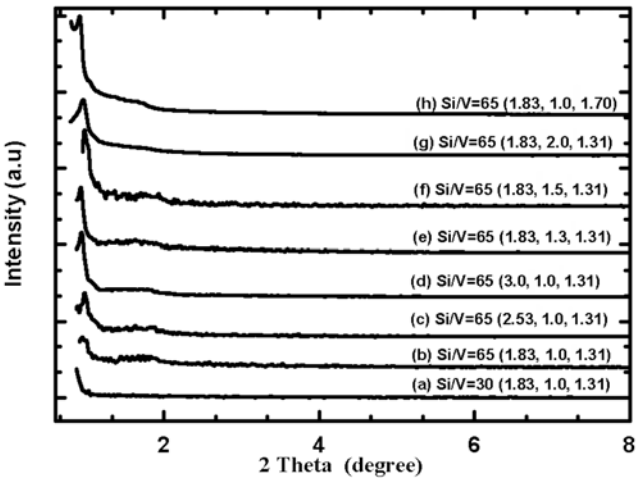

Fig. 1. XRD patterns for V-KIT-6 synthesized using 0.017 P123/1.83-3.0 HCl/1.0-2.0 TEOS/1.31-1.70 BuOH/195 H_2O.

1. XRD of V-KIT-6 (65) Synthesized at Different Molar Ratios of HCl and TEOS

Fig. 1(a)-(h) shows the powder XRD patterns of the V-KIT-6 synthesized under various conditions. Table 1 shows the textural property of the materials. The increase in the molar ratio of HCl in the starting gel (HCl/TEOS=1.83→3.0) improved the structural order (Fig. 1(b)-(d)). Although V-KIT-6 (65) synthesized at an HCl molar ratio of 1.83 produced an XRD pattern with the (211) reflection, the peak lacked intensity and higher order peaks were not well resolved. This suggests that at this HCl content, vanadium intrusion causes structural irregularity. As the HCl concentration was increased to 2.53 and 3.00, the quality of the cubic phase improved. The *d*-spacing was found to reach a maximum at an HCl molar ratio 3.0, suggesting significant vanadium incorporation. The unit cell (a_0) was found to be high with a pronounced wall thickness (Table 1).

To tune the rate of silica hydrolysis and condensation, the amount of TEOS, and BuOH was varied from 1.0-2.0/1.31-1.70, respectively, at 373 K for 24 h with the vanadium molar ratio 0.40 and HCl molar ratio 3.0 (Fig. 1(e)-(h)). Increasing the amount of the silica from 1.0 to 1.3 produced a diffraction pattern with improved structural ordering. The *d*-spacing was found to be high of about 95 Å. The wall thickness evaluated using $ds=a_0/2-w_{BJH}$ was found to be about 5.7 nm, where, a_0 is the XRD unit cell parameter, while w_{BJH} is the pore diameter calculated by using the BJH method. However, a further increase in the silica mole ratio to 1.5 and 2.0 clearly showed a transition from a well ordered Ia3d phase to a poorly ordered cubic phase (Fig. 1(f) and (g)). The XRD intensities decreased and the structural order reflected a weakening of the (211) reflection. The higher order peaks in the region 2θ=1-2 also disappeared. The wall thickness decreased to 4.7 nm. Therefore, the TEOS molar ratio was fixed at 1.0, and the influence of the *n*-butanol content was then examined. Increasing the amount of butanol from 1.30 to 1.70 resulted in a decreased structural ordering of KIT-6. Although the intensity of the peak increased, it lacked cubic (211) order reflection.

2. Nitrogen Adsorption Isotherm for VKIT-6 (65) Synthesized at Different Molar Ratios of HCl and TEOS

Table 1. Textural properties of KIT-6 (65) at different HCl, TEOS and BuOH mole ratio with a gel composition of 0.017 P123/1.0-2.0 TEOS/1.31-1.70 BuOH/1.83-3.0 HCl/195 H_2O

Synthetic condition in molar ratio			d_{211}	a_0	Surface area	Pore size	Pore volume	d
HCl	TEOS	BuOH	(Å)	(nm)	(m^2/g)	BJH_{adsorp} (nm)	BJH_{adsorp} (cm^3/g)	(nm)
1.83[a]	1.0	1.31	-	-	18.5	23.6	0.10	-
1.83	1.0	1.31	89.3	21.8	857	6.0	0.82	4.9
2.53	1.0	1.31	91.1	22.3	875	5.0	1.10	6.1
3.00	1.0	1.31	95.0	23.2	902	5.7	1.00	5.9
3.00	1.3	1.31	94.6	23.1	916	5.7	1.18	5.8
3.00	1.5	1.31	91.1	22.3	717	5.4	0.83	5.7
3.00	2.0	1.31	91.1	22.3	596	6.4	1.00	4.7
1.83	1.0	1.70	96.1	23.5	791	4.7	0.81	7.0

[a]Si/V=30 synthesized before optimization study; XRD unit cell parameter (a_0) is calculated using the formula $a_0=6^{1/2}\ d_{211}$; The wall thickness (d) evaluated using $d=a_0/2-w_{BJH}$, where w_{BJH} is the pore diameter calculated using the BJH method

The nitrogen adsorption isotherm for KIT-6 with Si/V=30, which was synthesized at a HCl molar ratio of 1.83, before the optimization study, did not feature steps of capillary condensation in the mesopores, as shown in Fig. 2(a). This confirmed the destruction of the material with a tremendous decrease in surface area (Table 1(a)). The surface area was only 18.5 m^2/g with a pore size distribution centered at 23.6 nm! The destruction of the pores eventually led to a very low pore volume of approximately 0.1 cm^3g^{-1}. This evolution probably corresponds to the mechanism of collapse of the interpenetrating continuous networks of chiral channels with an increase in the metal content leading to the large disordered cavities, and thereby decreasing the surface exposed to N_2 [17]. The gradual collapse of the silica pore walls generated new larger pores with varying sizes, which broadened the pore size distribution with its center shifting to much larger values. This demonstrates the importance of optimizing the acidity for vanadium incorporation.

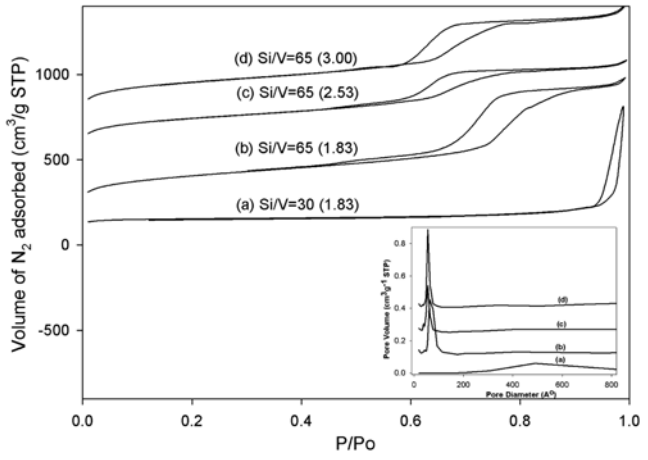

Fig. 2. N_2 adsorption-desorption isotherms for V-KIT-6 (65) samples synthesized at different pH, with composition of 0.017 P123/1 TEOS/1.31 BuOH/x HCl/195 H_2O. The molar ratio of HCl (x) varied as (a) Si/V=30 (1.83) (b) Si/V=60 (1.83) (c) Si/V=60 (2.53) and (d) Si/V=60 (3.00), respectively. The pore size was analyzed with the adsorption branch using the BJH algorithm.

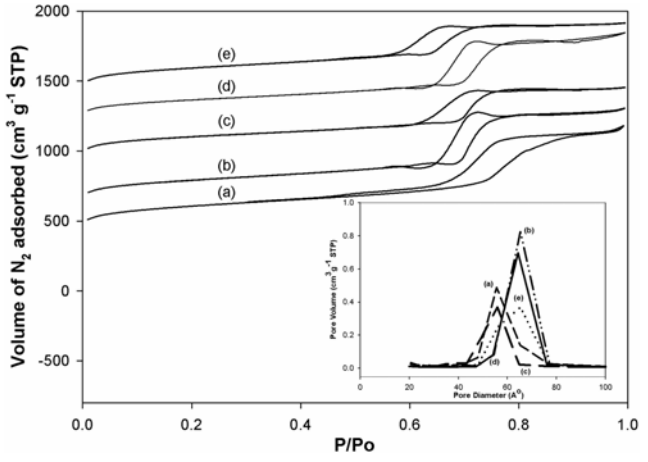

Fig. 3. N_2 adsorption-desorption isotherms for V-KIT-6 (65) samples synthesized at different TEOS and BuOH concentrations, with composition of 0.017 P123/x TEOS/y BuOH/1.83 HCl/195 H_2O. The molar ratio of TEOS (x) and BuOH (y) varied as (a) 1.0, 1.31 (b) 1.3, 1.31 (c) 1.5, 1.31 (d) 2.0, 1.31 and (e) 1.0, 1.70, respectively.

Fig. 2(b)-(d) shows the nitrogen adsorption-desorption isotherm for Si/V=65 with gradual increases in the HCl molar ratio from 1.83 to 3.00. At an HCl molar ratio of 1.83, the nitrogen adsorption-desorption isotherm showed a relatively broad hysteresis loop, which did not close even at relative pressures ≤0.6 (Fig. 2(b)). As the HCl molar concentration was increased to 3.0, the sharpness and height of the capillary condensation step in the isotherms improved with pore size uniformity (Fig. 2(c)). Fig. 3 shows the nitrogen adsorption-desorption isotherms measured for the samples with increasing TEOS/ BuOH molar ratio in the range 1.0-2.0/1.31-1.70 at the fixed HCl concentration 3.0. The increase in TEOS concentration to 1.3 resulted in a typical H1 hysteresis loop, indicating channel-like pores with a pronounced capillary condensation step, which is a characteristic of high-quality large pore mesoporous materials.

Fig. 4(a) and (b) clearly shows the influences of these three variables (HCl, TEOS and BuOH) on the textural properties of V-KIT-6. The increase in the HCl molar ratio from 1.83 to 3.0 resulted in a gradual increase in surface area. As shown in Table 1, the surface

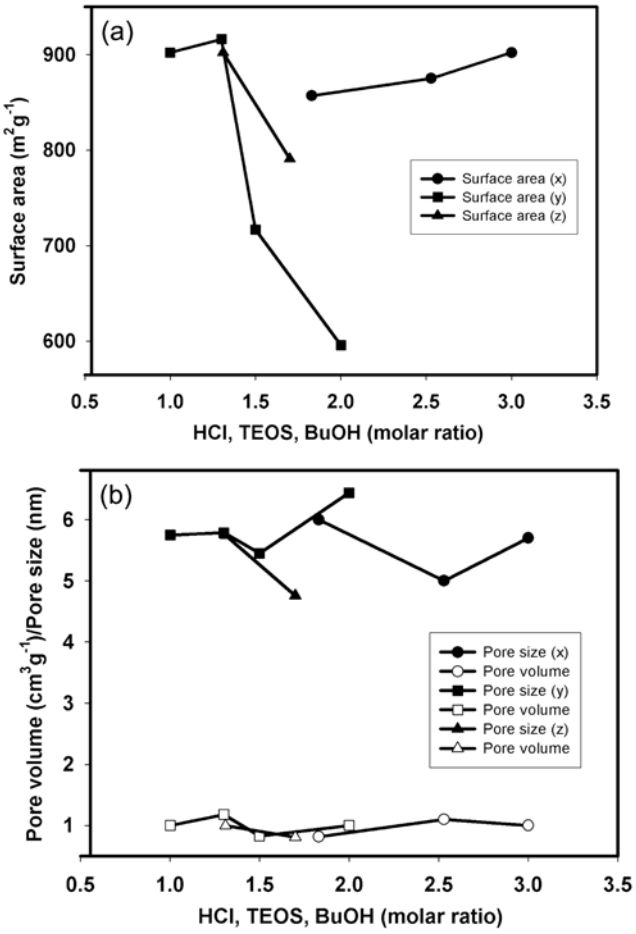

Fig. 4. Influence of HCl, TEOS, and BuOH molar ratio on the surface area, pore size and pore volume of V-KIT-6 (65) with the gel composition of 0.017 P23/x HCl/y TEOS/z BuOH/ 195 H_2O. The molar ratio varied as for HCl (x=1.83, 2.53, 3.0), TEOS (y=1.0, 1.3, 1.5, 2.0) and BuOH (z=1.31, 1.70).

area increased to the maximum of 902 m^2g^{-1} at HCl mole ratio 3.0. On the other hand, at a fixed HCl content of 1.83, the surface area increased from 902 m^2g^{-1} to 916 m^2g^{-1} with increasing TEOS content from 1.0 to 1.3, which then decreased to 717 m^2g^{-1} and 596 m^2g^{-1} as the TEOS molar ratio was further increased to 1.5 and 2.0, respectively. The change in butanol content from 1.31 to 1.70 did not improve the textural property because it only reduced the surface area from 902 to 791 m^2g^{-1}. Fig. 4(b) shows the influence of the HCl and TEOS molar ratio on the pore size and pore volume. The pore size decreased slightly from 6.0 to 5.7 nm, with increasing HCl content from 1.83 to 3.0. The trend reversed when the TEOS content was increased at a fixed HCl molar ratio 1.83, where the pore size increased from 6.0 to 6.4 nm. The change in butanol content from 1.3 to 1.7 reduced the pore size from 6.0 to 4.7 nm. The pore volume generally remained in the range of 0.8 to 1.0 cm^3g^{-1}.

3. Optimization of Synthesis Time and Temperature for V-KIT-6 (65)

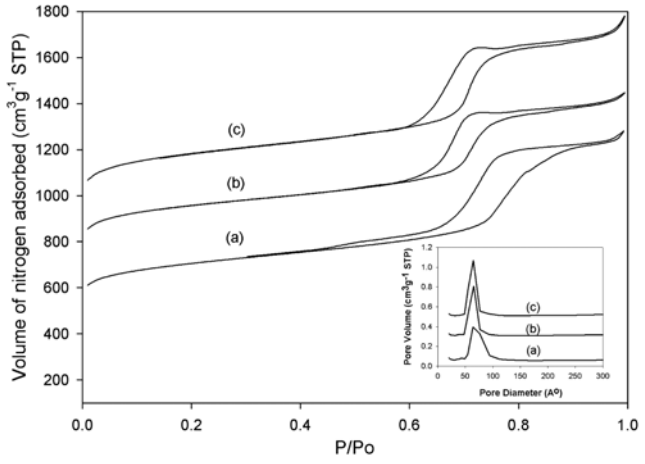

Fig. 5. N_2 adsorption-desorption isotherms for V-KIT-6 (65) samples synthesized at different stirring time (a) 24 h (b) 36 h and (c) 48 h, with the gel composition of 0.017 P123/1.0 TEOS/ 1.31 BuOH/1.83 HCl/195 H_2O.

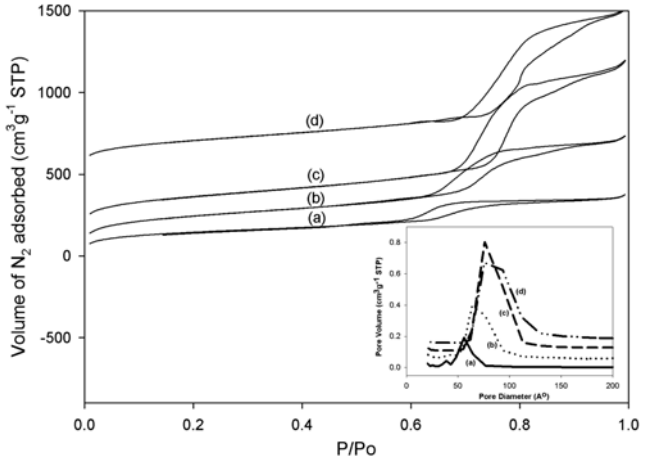

Fig. 6. N_2 adsorption-desorption isotherms for V-KIT-6 (65) samples synthesized at different hydrothermal condition (a) 80 °C (b) 100 °C (c) 120 °C and (d) 130 °C, with the gel composition of 0.017 P123/1.0 TEOS/1.31 BuOH/1.83 HCl/195 H_2O.

Table 2. Textural properties of KIT-6 (65) synthesized under various hydrothermal conditions and stirring times with a gel composition of 0.017 P123/1.3 TEOS/1.31 BuOH/3.0 HCl/195 H_2O

Hydrothermal condition (°C)	Stirring time (h)	Surface area (m^2/g)	Pore size BJH_{adsorp} (nm)	Pore volume BJH_{adsorp} (cm^3/g)
80	24	686	4.9	0.58
100	24	875	5.1	1.10
120	24	941	7.9	1.73
130	24	745	8.5	1.59
100	36	914	5.9	1.10
100	48	1009	6.2	1.32

Mesoporous materials are usually synthesized under hydrothermal conditions at temperatures ≥100 °C. During the hydrothermal process, the dissociation of metal-O-Si bonds becomes easy under acidic conditions [18]. Hence the synthesis condition can be tuned by optimizing stirring time (24-72 h) and hydrothermal condition (80-130 °C). Fig. 5 and 6 show the isotherm pattern. All the samples showed a characteristic isotherm pattern that is typical cubic structure for KIT-6. Table 2 shows surface area, pore size and pore volume at different stirring time and hydrothermal condition. The increase in stirring time from 24 h to 36 h ameliorated the surface area from 875 to 914 m^2/g. This shows that in order to achieve a state of equilibrium, sufficient time (≥24 h) is needed to allow optimal condensation. The optimum stirring time was found to be 48 h, which produced a material with the highest surface area at approximately 1,009 m^2/g, with a medium pore size of 6.2 nm. It means that the optimized prolonged intermicellar condensation of silica favors improved textural properties. An increase in the hydrothermal conditions from 80 °C to 120 °C increased the surface area from 686 m^2/g to 941 m^2/g. Further increases in temperature to 130 °C resulted in a decrease in surface area to 745 m^2/g. This can be viewed by direct observation of the isotherms shown in Fig. 6, where there is a gradual shift in the position of the capillary condensation from a relative pressure of 0.65 to a higher partial pressure. There was an increase in mesopore size from 4.9 to 8.5 nm with increasing temperature from 80 to 130 °C. KIT-6 synthesized at 130 °C contained mesopores with a wider pore size distribution and a large average pore diameter of approximately 8.5 nm. The pore volumes increased significantly from 0.58 to 1.59 cm^3/g with increasing temperature from 80 to 130 °C. The improvement obtained by the hydrothermal treatment was attributed to the further condensation and reorganization of the mesoporous framework [19].

4. Optimization of Vanadium Content

The amount of vanadium influenced the framework structure and crystallinity of the Ia3d phase significantly. Therefore, in order to improve the stability of V-KIT-6 with good structural ordering, it is essential to carefully control the vanadium content. Fig. 7(a)-(h) shows the powder X-ray diffraction patterns of the calcined V-KIT-6 samples at various Si/V molar ratios using the gel composition 0.017 P123/0.08-2.40 V/1.3 TEOS/1.31 BuOH/3.0 HCl/195 H_2O. The gel was stirred for 48 h at 373 K. The XRD patterns of the calcined cubic mesoporous materials Fig. 7(b)-(g) show excellent structural order with the symmetry being commensurate with the body-

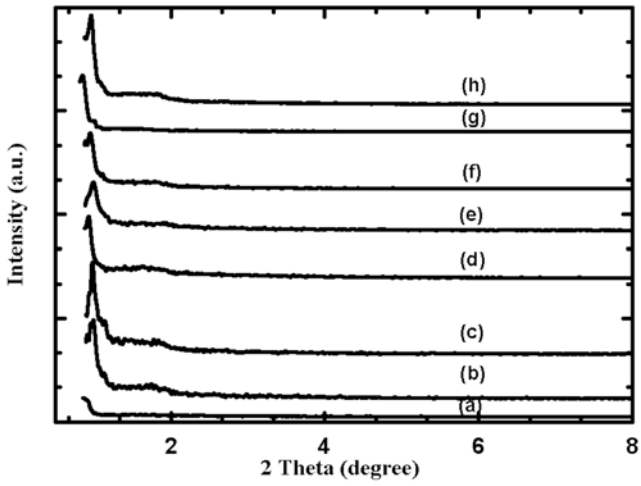

Fig. 7. Powder XRD patterns for the calcined V-KIT-6 mesostructured materials with various Si/V ratios using 0.017 P123/1.3 TEOS/1.31 BuOH/3.0 HCl/195 H_2O. (a) Si/V=5 in gel (b) Si/V=11 (c) Si/V=49, (d) Si/V=65 (e) Si/V=212 (f) Si/V=305 (g) as-synthesized V-KIT-6 (305) (h) Si-KIT-6.

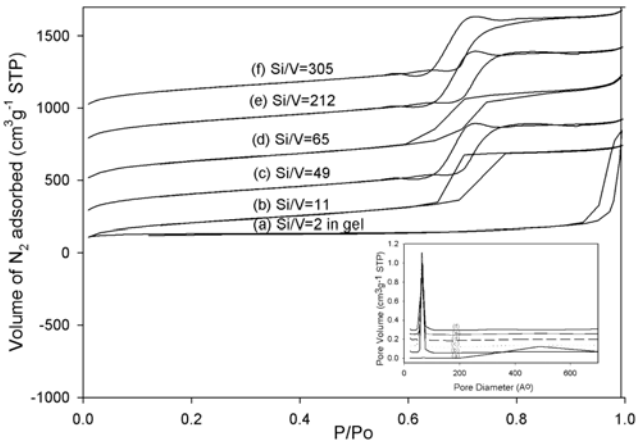

Fig. 8. N_2 adsorption-desorption isotherms for cubic Ia3d V-KIT-6 samples synthesized with different Si/V ratios with the gel composition of 0.017 P123/1.3 TEOS/1.31 BuOH/3.0 HCl/195 H_2O. The Si/V molar ratios varied as (a) Si/V=2 in gel (b) Si/V=11 (c) Si/V=49 (d) Si/V=65 (e) Si/V=212 and (f) Si/V=305, respectively.

centered cubic Ia3d space group matching well with the reported data [20]. The structural orderness was confirmed by the XRD patterns of the calcined materials, showing basal peaks corresponding to (211) at $2\theta \approx 1^{o}$ with several higher order reflections in the region 2θ=1.5-2. A gradual increase in the amount of V resulted in a decrease in the intensity of the higher order peaks. This might be due to the destructive interference of the mesoscopic order with increasing amount of vanadium species. As the amount of V incorporation increased, the basal diffraction peak (211) of the as-synthesized KIT-6 material shifted considerably towards a lower 2θ value around 0.8°. This increase in basal plane spacing compared with its pure silica analogue confirms the presence of vanadium in the silicate framework. This is consistent with what would be expected because the V-O bond length is longer than the Si-O bond length [21].

As shown in Table 3, the unit cell parameter of the cubic mesophase calculated by using the formula $a_o=6^{1/2}d_{211}$ was approximately 21.8-23.1 nm. The increase in unit cell indicates the insertion of a heteroatom and a thickening of the pore wall through transition metal promoted cross-linking of the amorphous silica walls [22]. The combination of the pore wall thickening and enlargement of the unit cell is a good indication for an actual incorporation of V centers. The wall thickness remained at approximately 5 nm, which might eventually lead to relatively high vanadium content in the mesopores. Therefore, the desired amount of metal can be inserted into KIT-6 by optimizing these three parameters. As measured by ICP-OES, the optimization yielded the incorporation of a vanadium metal content ranging from 0.37 to 4.9 wt%. The Si/V ratios measured by XRF (Table 3) show that a comparable amount of vanadium taken in the initial gel mixture was incorporated into the framework. The incorporated metal content was higher than those in earlier reports and it was obtained with a shorter synthesis time. However, further increasing the vanadium to Si/V=5 in the synthesis gel resulted in the destruction of the material irrespective of the conditions used (Fig. 7(a)).

Fig. 8 shows the nitrogen adsorption of V-KIT-6 at Si/V ratios ranging from 11 to 305. The KIT-6 materials exhibited type IV isotherms accompanied by much steeper steps of capillary condensation. The presence of an H1 hysteresis loop shows that all the samples have good mesopore structural ordering and a relatively narrow pore size distribution. The synthesized V-KIT-6 materials showed a relatively high surface area ranging 712-1,036 m^2/g with the pore size varied from 5.2 to 5.8 nm. The pore volume was upto 1.37 cm^3/g. The wall thickness was around 5.4 nm. The HRTEM images of the V-KIT-6 (11) obtained confirm the presence of large domains of a 3-D silica-vanadia network, which highlights the interconnec-

Table 3. Textural properties of KIT-6 synthesized with various Si/V ratios with a gel composition of 0.017 P123/1.3 TEOS/1.31 BuOH/3.0 HCl/195 H_2O at 100 °C

Catalysts	Si/V in gel	ICP (wt%)	d_{211} (Å)	a_0 (nm)	Surface area (m^2/g)	Pore size BJH_{adsorp} (nm)	Pore volume BJH_{adsorp} (cm^3/g)	d (nm)
V-KIT-6	5	-	-	-	42.3	40.7	0.23	-
V-KIT-6 (11)	10	4.95	93.0	22.7	712	6.0	1.17	5.3
V-KIT-6 (49)	40	1.89	91.1	22.3	691	6.0	1.10	5.1
V-KIT-6 (65)	60	1.74	94.6	23.1	916	5.7	1.19	5.8
V-KIT-6 (212)	200	0.46	90.2	22.0	1036	5.8	1.37	5.2
V-KIT-6 (305)	300	0.32	89.3	21.8	837	5.7	1.24	5.2

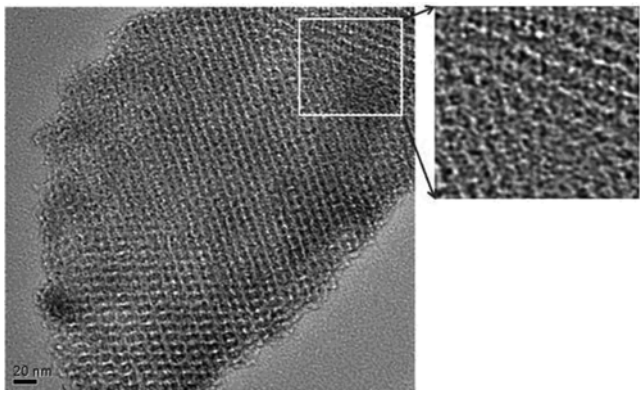

Fig. 9. TEM spectra for calcined V-KIT-6 sample with Si/V=11.

tivity in the pore structure of the Ia3d cubic phase (Fig. 9). As the vanadium content in the synthesis gel was increased to Si/V=5, the cubic phase collapsed leading to an amorphous phase, irrespective of the condition used.

CONCLUSION

The effects of the various synthesis parameters, such as the amount of HCl, TEOS, BuOH, and synthesis time and temperature, on the properties of the cubic KIT-6 for vanadium incorporation were investigated systematically. The vanadium incorporated KIT-6 showed the presence of highly dispersed vanadium with a very high surface area (~1,000 m^2/g). The pore size distribution varied within a narrow range between 5.7 to 6.0 nm with a wall thickness of approximately 5.8 nm at the maximum. A detailed reactivity study of the V-KIT-6 catalysts will be carried out as a next series of this work and the results will be published in the near future.

ACKNOWLEDGMENT

The study was supported by Korea Science and Engineering Foundation (R01-2007-000-10183-0), and Brain Korea 21 Project. The authors are grateful to KBSI for performing characterization studies.

REFERENCES

1. W. Zhang, J. Wang, P. T. Tanev and T. Pinnavaia, *J. Chem. Soc.*, *Chem. Commun.*, 979 (1996).
2. K. M. Reddy, I. Moudrakaski and A. J. Sayari, *J. Chem. Soc.*, *Chem. Commun.*, 1059 (1994).
3. S. Gontier and A. Tuel, *Microporous Mater.*, **5**, 161 (1995).
4. Z. Luan, E. M. Maes, P. A. W. Van der Heide, D. Zhao, R. S. Czernuszewicz and L. Kevan, *Chem. Mater.*, **11**, 3680 (1999).
5. Z. Luan, J. Y. Bae and L. Kevan, *Chem. Mater.*, **12**, 3202 (2000).
6. F. Gao, Y. Zhang, H. Wan, Y. Kong, X. Wu, L. Dong, B. Li and Y. Chen, *Micro. Meso. Mater.*, 2007, doi:10.1016/j.micromeso.2007.06.041.
7. R. Murugavel and H. W. Roesky, *Angew. Chem., Int. Ed.*, **109**, 44491 (1997).
8. J. Fan, C. Yu, L. Wang, B. Tu, D. Zhao, Y. Sakamoto and O. Terasaki, *J. Am. Chem. Soc.*, **123**, 12113 (2001).
9. Y. Sakamoto, M. Kaneda, O. Terasaki, D. Y. Zhao, J. M. Kim, G. D. Stucky, H. Y. Shin and R. Ryoo, *Nature*, **408**, 449 (2000).
10. M. S. Morey, A. Davidson and G. D. Stucky, *J. Porous Mater.*, **5**, 195 (1998).
11. T. W. Kim, F. Kleitz, B. Paul and R. Ryoo, *J. Am. Chem. Soc.*, **127**, 7601 (2005).
12. Y.-W. Chen and Y.-H. Lu, *Ind. Eng. Chem. Res*., **38**, 1893 (1999).
13. S. Lim and G. L. Haller, *J. Phys. Chem. B*, **106**, 8437 (2002).
14. G. Du, S. Lim, Y. Yang, C. Wang, L. Pfefferle and G. L. Haller, *Appl. Catal. A. Gen.*, **302**, 48 (2006).
15. S. E. Dapurkar, A. Sakthivel and P. Selvam, *J. Mol. Catal. A-Chem.*, **223**, 241 (2004).
16. P. Selvam and S. E. Dapurkar, *Appl. Catal. A: Gen*., **276**, 257 (2004).
17. A. Galarneau, M.-F. Driole, C. Petitto, B. Chiche, B. Bonelli, M. Armandi, B. Onida, E. Garrone, F. Renzo and F. Fajula, *Micro. Meso. Mater.*, **83**, 172 (2005).
18. W.-H. Zhang, J. Lu, B. Han, M. Li, J. Xiu, P. Ying and C. Li, *Chem. Mater.*, **14**, 3413 (2002).
19. P. Van Der Voort, M. Mathieu, F. Mees and E. F. Vansant, *J. Phys. Chem. B*, **102**, 8847 (1998).
20. A. Vinu, S. Anandan, C. Anand, P. Srinivasu, K. Ariga and T. Mori, *Micro. Meso. Mater.* 2007, doi:10.1016/j.micromeso.2007.05.037.
21. S. Shylesh and A. P. Singh, *J. Catal.*, **233**, 359 (2005).
22. M. Mathieu, P. Van Der Voort, B. M. Weckhuysen, R. R. Rao, G. Catana, R. A. Schoonheydt and E. F. Vansant, *J. Phys. Chem. B*, **105**, 3393 (2001).